DOI: 10.61782/fa.2025.0179

FORUM ACUSTICUM EURONOISE 2025

BLOOD-BRAIN BARRIER OPENING IN SMALL ANIMALS USING FOCUSED ULTRASOUND

Jesús Limens-Pinaque[2*] **Josep Rodríguez-Sendra**[1] **Juan J. Rodríguez-García**[1]
Adrián Arándiga[1] **Jose L. Alonso-Ramos**[1] **Daniel Panadero-Soler**[2]
Noé Jiménez[1] **Patricia Rico**[3,4] **Santiago Canals**[2] **Francisco Camarena**[1*]

[1] Instituto de Instrumentación para Imagen Molecular (I3M), Universitat Politècnica de València (UPV) - Consejo Superior de Investigaciones Científicas (CSIC), Spain
[2] Instituto de Neurociencias (IN), Universidad Miguel Hernández (UMH) - Consejo Superior de Investigaciones Científicas (CSIC), Spain
[3] Centre for Biomaterials and Tissue Engineering (CBIT), Universitat Politècnica de València (UPV), Spain
[4] Biomedical Research Networking Center in Bioengineering, Biomaterials and Nanomedicine (CIBER-BBN), Spain

ABSTRACT

Focused ultrasound combined with microbubbles can locally and transiently open the blood-brain barrier (BBB) in a non-invasive and safe manner, providing a potential strategy for drug delivery into the brain. The technique is currently being used to test drugs for the treatment of different pathologies; however, the BBB opening dimensions depends on several characteristics of the ultrasonic beam. In this work we characterize the BBB opening in small animals produced by a manufactured transducer operating at frequencies 1.05 MHz (fundamental; $FWHM_{3dB}$ = 1.5 mm | DOF_{3dB} = 6 mm) and 3.25 MHz (first harmonic; $FWHM_{3dB}$ = 0.5 mm | DOF_{3dB} = 2 mm). The transducer has been tested in 11 mice, demonstrating its capability for different BBB opening dimensions with gadolinium (Gd) signal detected in contrast-enhanced T1-weighted MRI.

Keywords: *ultrasound, blood-brain barrier opening, preclinical research, neuromodulation, drug delivery*

[*] ***Corresponding authors***: *jlimens@umh.es fracafe@fis.upv.es*

1. INTRODUCTION

The blood-brain barrier is a highly selective structure that regulates the passage of substances from the blood into the central nervous system (CNS). It is composed mainly of specialized endothelial cells, linked by tight junctions, which limit the diffusion of molecules larger than 400-500 Da and maintain brain homeostasis. However, this protective barrier also restricts the passage of most therapeutic compounds, posing a significant challenge for drug delivery in both preclinical animal models and clinical applications in humans.

Focused ultrasound (FUS) combined with microbubbles has been proven to transiently, non-invasively, and safely open the BBB in a localized manner [1]. This technique has been successfully demonstrated in various species, including rodents [2,3], macaques [4,5], and humans [6,7], enabling targeted drug delivery to the brain. Moreover, BBB opening has been explored for various applications, including enhanced chemotherapy delivery, gene therapy, and the treatment of neurodegenerative disorders [8].

In this study, we will use a manufactured FUS transducer operating at frequencies 1.05 (fundamental) and 3.25 MHz (first harmonic) together with microbubbles to open the

BBB in n = 20 mice. By employing T1-weighted FLASH magnetic resonance imaging (MRI) with gadolinium contrast, we will verify and analyze the openings.

2. MATERIALS AND METHODS

2.1 Acoustic simulation

Acoustic simulation was performed using the k-Wave MATLAB toolbox to model ultrasound wave propagation and quantify pressure distribution, focal spot localization, and transmission efficiency through the skull [9]. The transducer utilized in the simulation was identical to the one employed in the experiment, operating in two modes: at its fundamental frequency of 1.05 MHz and at its first harmonic frequency of 3.25 MHz. It had a diameter of 65 mm, a focal length of 50 mm, an inner aperture of 4 mm and a thickness of 2 mm.

For the acoustic simulations, we used an isotropic numerical grid with a spatial step of Δh = 292 µm for simulations at 1.05 MHz and Δh = 74 µm for simulations at 3.25 MHz, corresponding to a spatial resolution of 6 grid points per wavelength at each frequency. The numerical time step was chosen to ensure a Courant-Friedrichs-Lewy (CFL) number of 0.25. The CT data of the mouse used for the simulation were identical to [10]. The density and speed of sound for each voxel were derived from converting the corresponding Hounsfield Units (HU) to acoustic impedance [11,12]. Acoustic absorption coefficients were obtained from [10] and were 0.0023, 0.4374, and 17.6946 dB/cm for water, brain, and bone, respectively, at 1.05 MHz, and 0.0072, 1.3540, and 54.7469 dB/cm for water, brain, and bone, respectively, at 3.25 MHz.

Figure 1 presents the normalized acoustic fields obtained from simulations, illustrating the acoustic field for both frequencies.

2.2 Acoustic characterization

Acoustic characterization was performed in a water tank filled with degassed water to characterize the ultrasound field parameters. The transducer was positioned using a motorized stage (15 µm resolution, PI miCos GmbH, Germany) to ensure precise alignment. A calibrated hydrophone (HNA-400, Onda Corporation, USA) with a preamplifier (AG-2010, Onda Corporation, USA) was used to measure pressure waveforms at various spatial locations inside the skull cavity. The experimental measurements taken in the pool were compared with the simulations to verify the consistency and validity of the results (Figure 1 Bottom subplots).

Measurements performed in the water tank using ex vivo tissue revealed that the attenuation of the mouse skull was 21% at 1.05 MHz and 52% at 3.25 MHz. At 1.05 MHz, an input signal of 150 mV was required to obtain a pressure of 0.5 MPa, while at 3.25 MHz, an input signal of 315 mV was required to achieve a pressure of 0.6 MPa. For all measurements, the exact system used in the in vivo experiments was employed (Figure 2).

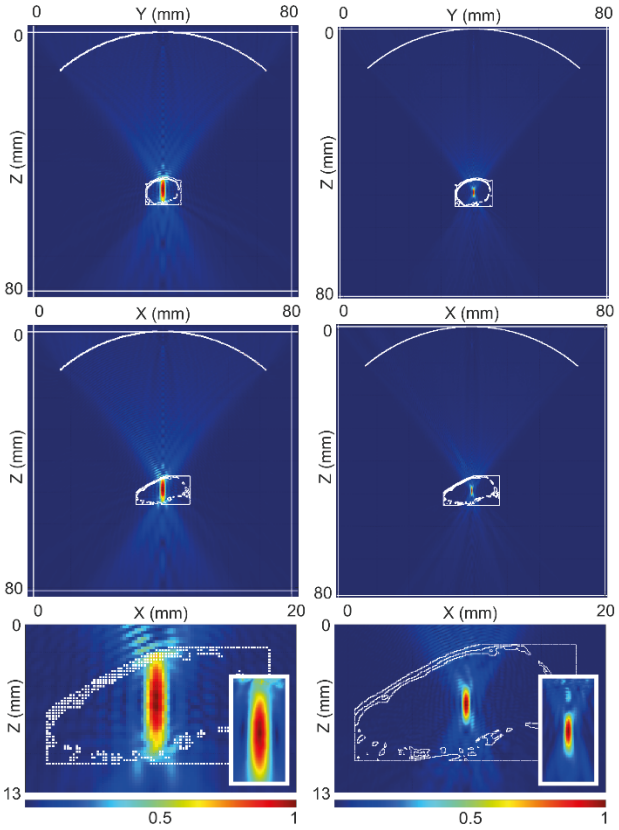

Figure 1. Ultrasound field simulated at 1.05 MHz (left), and 3.25 MHz (right). Images at the bottom show a zoom view of the focal point along with a subplot with the experimental results.

2.3 Animals

A total of 20 female swiss mice (age: 8 weeks, weight: 20 g) (SN-SWISS-F, JANVIER LABS, France) were used in this study. The animals were housed in standard conditions with a 12-hour light/dark cycle, temperature between 20 and 24°C and ad libitum access to food and water. When needed during the experiment, mice were anesthetized with 1-2% isoflurane and their body temperature was maintained at 37°C using a heating pad.

All procedures were conducted in accordance with European Directive 2010/63/EU on the protection of animals used for scientific purposes and approved by the Conselleria de Agricultura, Ganadería y Pesca of the Generalitat Valenciana (Approval ID: 2022 VSC PEA 0254 tipo 2).

2.4 Sonication

The sonication was performed using a custom ultrasound system based on a piezoelectric focal bowl, an arbitrary waveform generator (Red Pitaya 125-14, Red Pitaya US, USA) and an amplifier (OPAMP PA119, Apex Microtechnology, USA) specifically designed for the experiment (Figure 2). Prior to sonification, the animal was shaved in the head area and placed on the stretcher. Intravenous 1 µl/g microbubble injection (Definity, Lantheus Medical, USA) was administered immediately before the sonification.

Two sonification protocols were applied. The first involved f = 1.05 MHz, P = 0.5 MPa, PRF = 5 Hz, DC = 3%, and t = 120 s, and was applied to 10 mice. The second utilized f = 3.25 MHz, P = 0.6 MPa, PRF = 5 Hz, DC = 3%, and t = 120 s, and was applied to 10 mice. Following the sonification, an intraperitoneal injection of 200 µl Gd (Dotarem, Guerbet, France) was administered.

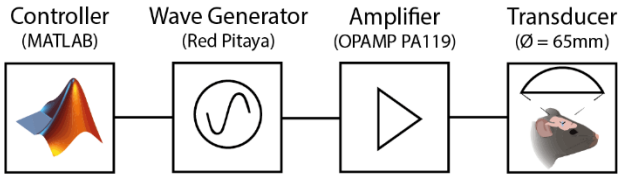

Figure 2. Ultrasound system diagram.

2.5 MRI

Mice were transferred to the MRI (BioSpec 70/30, Bruker, Germany) and anesthetized with isoflurane. A contrast-enhanced T1-weighted FLASH scan (TR/TE of 230/3.3 ms, flip angle of 70°, number of excitations of 18, inplane resolution of 85 µm × 85 µm, slice thickness of 500 µm and receiver bandwidth of 50 kHz.) was acquired 60 minutes after gadolinium injection. Scans were performed in both coronal and horizontal planes (Figure 3).

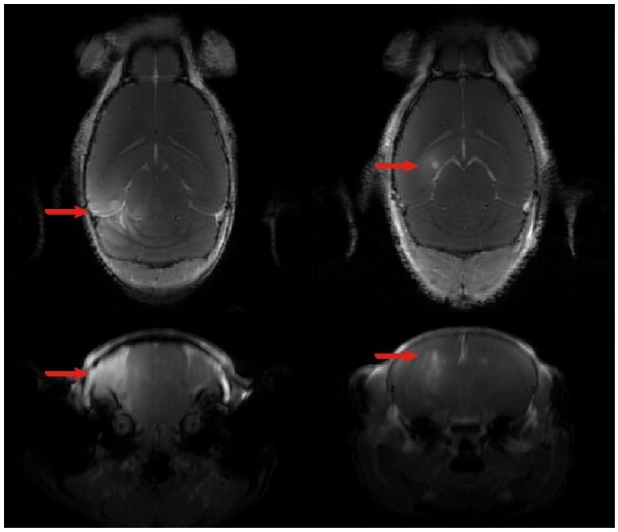

Figure 3. T1-weighted MRI images showing gadolinium due to blood-brain barrier opening. On the left, images obtained with the first protocol (f = 1.05 MHz), and on the right, with the second (f = 3.25 MHz).

2.6 BBB opening analysis

The analysis of the Gd signal in the T1-weighted MRI images aimed to obtain the centroid coordinates and the total volume of the BBB openings. For this analysis, *SAMson* was used to automatically segment the brain from the surrounding tissue in coronal planes [13]. Once isolated, all brains were segmented with *MATLAB* [14] using the same intensity threshold, resulting in a binary matrix. The *regionprops* function was then applied, which considers only the nonzero values in the matrix to extract the centroid coordinates (y and z coordinates). Additionally, the *nnz* function was used to count all nonzero voxels in the matrix. The total volume was then obtained by multiplying this

voxel count by the dimensions of a single voxel (85 µm × 85 µm × 500 µm). Since the *SAMson* tool is only applicable to coronal MRI studies, an additional manual segmentation was performed using *ITK-SNAP* [15] on the horizontal plane MRI study to obtain the *x* coordinates.

Finally, the centroid coordinates of each opening were referenced to the center of the generated matrix, as the matrix size had been adjusted to match the exact dimensions of the brain. This reference is robust across our different MRI studies, allowing for a reliable comparison of the locations of the openings.

3. RESULTS

Successful BBB opening was achieved in 11 mice. 9 mice did not show any opening. All of them had difficulty injecting the microbubbles. BBB disruption was observed in 6 mice using the 1.05 MHz protocol and in 5 mice using the 3.25 MHz protocol. For the first 7 openings (6 at 1.05 MHz and one at 3.25 MHz), the transducer was positioned in a specific brain region and kept fixed while the animals were placed accordingly to evaluate targeting precision. Subsequently, the transducer was shifted 3 mm forward to perform the remaining four openings at 3.25 MHz. The average BBB opening volume was 19.85 ± 6.20 mm³ for the 1.05 MHz condition and 12.41 ± 3.66 mm³ for the 3.25 MHz condition.

Regarding targeting precision, the displacement of the centroid of the BBB opening respect to the mean value per sonication event was 0.23 ± 0.18 mm, 0.20 ± 0.11 mm, and 0.07 ± 0.03 mm along the X, Y, and Z axes, respectively, for 1.05 MHz, and 0.08 ± 0.05 mm, 0.16 ± 0.13 mm, and 0.12 ± 0.06 mm along the X, Y, and Z axes, respectively, for 3.25 MHz (Figure 4). The total displacement of the centroid of all the BBB openings was 0.18 ± 0.16 mm, 0.17 ± 0.12 mm, and 0.11 ± 0.08 mm along the X, Y, and Z axes, respectively.

For the 1.05 MHz frequency, the positional analysis included all 6 mice with successful BBB openings. However, for the 3.25 MHz case, only three mice were considered for positional analysis. One of the remaining two was sonicated at the same location as the 1.05 MHz condition to confirm successful opening, while the other exhibited an opening significantly displaced from the intended area due to an animal positioning error. For the total displacement error, all BBB openings were included except the one with positioning error.

Additionally, for the 3.25 MHz case, all three openings were performed by physically shifting the target 3 mm forward to assess the system's targeting precision. The measured distances between these openings and the previous ones resulted in an average separation of 3.16 ± 0.11 mm.

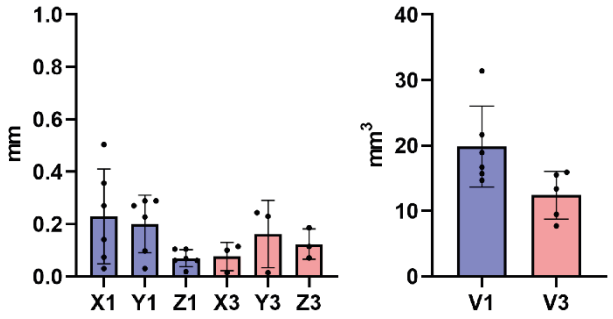

Figure 4. (Left) Mean and standard deviation of the absolute centroid displacement of the BBB opening along the X, Y, and Z axes. (Right) Mean and standard deviation of the volume of the BBB opening. Blue bars represent data acquired at 1.05 MHz, while red bars correspond to 3.25 MHz.

4. CONCLUSIONS

Twenty BBB opening procedures have been performed in mice using two different protocols in order to evaluate the capability of an FUS system to perform precise openings.

The average BBB opening volume was larger for the 1.05 MHz condition (19.85 ± 6.20 mm³) compared to the 3.25 MHz condition (12.41 ± 3.66 mm³), indicating a frequency-dependent effect on opening dimensions. Targeting precision analysis showed small centroid displacements per sonication event, with mean deviations of 0.23 ± 0.18 mm, 0.20 ± 0.11 mm, and 0.07 ± 0.03 mm along the X, Y, and Z axes, respectively, for 1.05 MHz, and 0.08 ± 0.05 mm, 0.16 ± 0.13 mm, and 0.12 ± 0.06 mm along the X, Y, and Z axes, respectively for 3.25 MHz. These results obtained are consistent and reliable, as they align with those described in

similar studies [10,16] and suggest that the manufactured transducer can achieve precise and reproducible targeting.

Furthermore, for the 3.25 MHz condition, the physical shift of the sonication target by 3 mm resulted in an observed average displacement of 3.16 ± 0.11 mm, confirming the system's targeting accuracy. This level of precision is particularly relevant for procedures requiring multiple BBB openings at different locations within the same experiment.

However, a significant portion of the variability in both volume and spatial distribution can be attributed to the initial target placement. Since the first sonications were performed at a randomly assigned location within the cerebellum due to errors in mice positioning, the irregular and smaller geometry of this brain region (compared to the hemispheres) led to Gd leakage spreading beyond the intended area, resulting in less well-defined openings. Quality of microbubble injections also played a crucial role in defining BBB opening volume, as incomplete administration of the microbubble dose frequently led to reduced opening sizes. Additionally, one case of significant displacement due to positioning error highlights the importance of accurate animal alignment in sonication experiments to ensure reproducibility and precise targeting across multiple sonication sites.

These findings demonstrate the feasibility of using the manufactured transducer for frequency-dependent BBB opening in small animals, providing valuable insights for future preclinical applications in drug delivery studies.

5. ACKNOWLEDGMENTS

This research has been funded by the Ministerio Español de Ciencia e Innovación y el Ministerio de Universidades with grant RYC2021-034920-I, PID2022-142719OB-C21 funded by MCIN/AEI/10.13039/501100011033/ and FEDER Una manera de hacer Europa and CNS2023-145707 and PRE2022-102801 funded by MCIN/AEI/10.13039/501100011033 and FSE+.

We would like to thank Juan José Manclús for providing us with a space in his laboratory to practice before the experiments, Juan González Valdivieso for his continuous assistance, Luis Tuset Sanchís for his technical support with the MRI, and Analía Rico Rodríguez for her assistance during the preliminary experiments. We also thank Sergio Jiménez Gambín for providing the mouse CT scan and Antonios Pouliopoulos for his advice on the execution of the blood-brain barrier opening.

6. REFERENCES

[1] Hynynen K, McDannold N, Vykhodtseva N, Jolesz FA. Noninvasive MR imaging-guided focal opening of the blood-brain barrier in rabbits. Radiology. 2001 Sep;220(3):640-6. doi: 10.1148/radiol.2202001804. PMID: 11526261.

[2] Kinoshita M, McDannold N, Jolesz FA, Hynynen K. Noninvasive localized delivery of Herceptin to the mouse brain by MRI-guided focused ultrasound-induced blood-brain barrier disruption. Proc Natl Acad Sci U S A. 2006 Aug 1;103(31):11719-23. doi: 10.1073/pnas.0604318103. Epub 2006 Jul 25. PMID: 16868082; PMCID: PMC1544236.

[3] Choi JJ, Pernot M, Small SA, Konofagou EE. Noninvasive, transcranial and localized opening of the blood-brain barrier using focused ultrasound in mice. Ultrasound Med Biol. 2007 Jan;33(1):95-104. doi: 10.1016/j.ultrasmedbio.2006.07.018. PMID: 17189051.

[4] Tung YS, Marquet F, Teichert T, Ferrera V, Konofagou EE. Feasibility of noninvasive cavitation-guided blood-brain barrier opening using focused ultrasound and microbubbles in nonhuman primates. Appl Phys Lett. 2011 Apr 18;98(16):163704. doi: 10.1063/1.3580763. Epub 2011 Apr 20. PMID: 21580802; PMCID: PMC3094460.

[5] McDannold N, Arvanitis CD, Vykhodtseva N, Livingstone MS. Temporary disruption of the blood-brain barrier by use of ultrasound and microbubbles: safety and efficacy evaluation in rhesus macaques. Cancer Res. 2012 Jul 15;72(14):3652-63. doi: 10.1158/0008-5472.CAN-12-0128. Epub 2012 May 2. PMID: 22552291; PMCID: PMC3533365.

[6] Carpentier A, Canney M, Vignot A, Reina V, Beccaria K, Horodyckid C, Karachi C, Leclercq D, Lafon C, Chapelon JY, Capelle L, Cornu P, Sanson M, Hoang-Xuan K, Delattre JY, Idbaih A. Clinical trial of blood-brain barrier disruption by pulsed ultrasound. Sci Transl Med. 2016 Jun 15;8(343):343re2. doi: 10.1126/scitranslmed.aaf6086. PMID: 27306666.

[7] Lipsman N, Meng Y, Bethune AJ, Huang Y, Lam B, Masellis M, Herrmann N, Heyn C, Aubert I, Boutet A, Smith GS, Hynynen K, Black SE. Blood-brain barrier opening in Alzheimer's disease using MR-guided focused ultrasound. Nat Commun. 2018 Jul 25;9(1):2336. doi: 10.1038/s41467-018-04529-6. PMID: 30046032; PMCID: PMC6060168.

[8] Gorick CM, Breza VR, Nowak KM, Cheng VWT, Fisher DG, Debski AC, Hoch MR, Demir ZEF, Tran NM, Schwartz MR, Sheybani ND, Price RJ. Applications of focused ultrasound-mediated blood-brain barrier opening. Adv Drug Deliv Rev. 2022 Dec;191:114583. doi: 10.1016/j.addr.2022.114583. Epub 2022 Oct 19. PMID: 36272635; PMCID: PMC9712235.

[9] Treeby BE, Cox BT. k-Wave: MATLAB toolbox for the simulation and reconstruction of photoacoustic wave fields. J Biomed Opt. 2010 Mar-Apr;15(2):021314. doi: 10.1117/1.3360308. PMID: 20459236.

[10] Jimenez-Gambin S, Jimenez N, Pouliopoulos A, Benlloch JM, Konofagou E, Camarena F. Acoustic Holograms for Bilateral Blood-Brain Barrier Opening in a Mouse Model. IEEE Trans Biomed Eng. 2022 Apr;69(4):1359-1368. doi: 10.1109/TBME.2021.3115553. Epub 2022 Mar 18. PMID: 34570701; PMCID: PMC9058858.

[11] Schneider U, Pedroni E, Lomax A. The calibration of CT Hounsfield units for radiotherapy treatment planning. Phys Med Biol. 1996 Jan;41(1):111-24. doi: 10.1088/0031-9155/41/1/009. PMID: 8685250.

[12] Mast, T.D. (2000). Empirical relationships between acoustic parameters in human soft tissues. *Acoustics Research Letters Online*, 1(2), 37–42.

[13] Panadero-Soler D, Kotb Selim M, Martínez-Tazo P, Muñoz-Moreno E, Ramos-Cabrer P, López-Larrubia P, De Santis S, Canals S, Pertusa, A. SAMson: an automated brain extraction tool for rodents using SAM. bioRxiv. 2025 Jan. doi: 10.1101/2024.03.07.583982

[14] The MathWorks, Inc. (2024). MATLAB (Version R2024b) https://www.mathworks.com

[15] Yushkevich PA, Piven J, Hazlett HC, Smith RG, Ho S, Gee JC, Gerig G. User-guided 3D active contour segmentation of anatomical structures: significantly improved efficiency and reliability. Neuroimage. 2006 Jul 1;31(3):1116-28. doi: 10.1016/j.neuroimage.2006.01.015. Epub 2006 Mar 20. PMID: 16545965.

[16] Hu Z, Chen S, Yang Y, Gong Y, Chen H. An Affordable and Easy-to-Use Focused Ultrasound Device for Noninvasive and High Precision Drug Delivery to the Mouse Brain. IEEE Trans Biomed Eng. 2022 Sep;69(9):2723-2732. doi: 10.1109/TBME.2022.3150781. Epub 2022 Aug 19. PMID: 35157574; PMCID: PMC9443669.